

Article

# Photooxidation of 2-(*tert*-Butyl)-3-Methyl-2,3,5,6,7,8-Hexahydroquinazolin-4(1*H*)-one, an Example of Singlet Oxygen *ene* Reaction †

Adrian Méndez, Jonathan Román Valdez-Camacho and Jaime Escalante \* 

The Center for Chemical Research, Autonomous University of Morelos State, Av. Universidad 1001, Chamilpa, Cuernavaca 62210, Mexico; 2009404340@uaem.mx (A.M.); valca@uaem.mx (J.R.V.-C.)

\* Correspondence: jaime@uaem.mx; Tel.: +52-777-329-7997

† Dedicated to Professor Eusebio Juaristi on the occasion of his 70th birthday.

Academic Editors: M. Graça P. M. S. Neves and Gianfranco Favi

Received: 7 September 2020; Accepted: 26 October 2020; Published: 29 October 2020



**Abstract:** Singlet oxygen *ene* reactions produce 2-(*tert*-butyl)-4a-hydroperoxy-3-methyl-2,4a,5,6,7,8-hexahydroquinazolin-4(3*H*)-one quantitatively during diffusion crystallization of 2-(*tert*-butyl)-3-methyl-2,3,5,6,7,8-hexahydroquinazolin-4(1*H*)-one in *n*-hexane/CH<sub>2</sub>Cl<sub>2</sub> solvent mixture. To confirm this photo-oxidation, a <sup>1</sup>H-NMR study in CDCl<sub>3</sub> was performed with exposure to ambient conditions (light and oxygen), with neither additional reactants nor catalysts. A theoretical study at the B3LYP/6311++G\*\* level using the QST2 method of locating transition states suggests a two-step mechanism where the intermediate, which unexpectedly did not come from the peroxide intermediate, has a low activation energy.

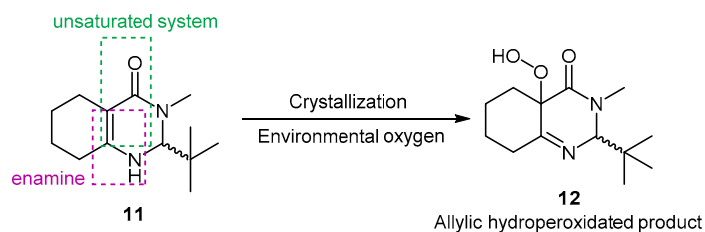
**Keywords:** singlet oxygen *ene* reaction; peroxidation; quinazolinone; singlet oxygen; intermediates; activation energy; transition state; reaction coordinate; B3LYP/6311++G\*\*; QST2 method; IRC calculations

## 1. Introduction

Molecular oxygen is a key agent in a variety of photooxidation processes [1,2]. As a reagent, there are mainly three pathways to incorporate molecular oxygen into the product: (1) by the triplet <sup>3</sup>O<sub>2</sub>, which plays the role of a radical scavenger agent; (2) by the superoxide radical anion generated through a single electron transfer (SET) process; and (3) by the singlet <sup>1</sup>O<sub>2</sub> which is usually produced through the energy transfer between the excited photocatalyst and <sup>3</sup>O<sub>2</sub> [3,4]. Photooxidative reactions involve initial light absorption by so-called photosensitizers, which then transfer the absorbed energy to other molecules, including dissolved oxygen (<sup>3</sup>O<sub>2</sub>) [5–7]. Olefins containing allylic hydrogen could form allylic hydroperoxides under the action of singlet oxygen [8,9]. Direct and selective oxygenation of C-H bonds to C-O bonds are still associated with challenges, such as harsh reaction conditions, as well as the use of expensive transition metal catalysts and the use of oxidant reagents in stoichiometric amounts. If these reactions can be achieved using metal-free catalysts, this could contribute to the development of green chemistry [10–12]. In this way, singlet molecular oxygen <sup>1</sup>O<sub>2</sub> plays a growing role in many processes. For example, the <sup>1</sup>O<sub>2</sub>-mediated allylic oxidation was used as an essential step in the synthesis of natural products or their synthetic analogues [13]. Although this reaction has been studied for many years, its mechanistic details are still a matter of debate either by theoretical or experimental results [13].

Herein we report a hydroperoxidated product (**12**) by a spontaneous photooxidation where hexahydroquinazolinone (**11**) is crystallized by overnight diffusion in an *n*-hexane/CH<sub>2</sub>Cl<sub>2</sub> (80:20) solvent mixture, Scheme 1. The scheme makes use of oxygen in the environment and at the same time

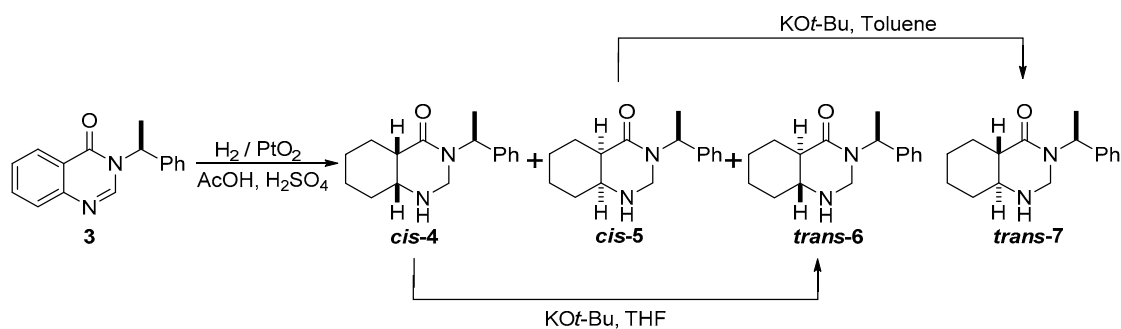
is able to avoid the use of photosensitizers (metallic catalysts or natural colorants), which is a constant challenge [14,15].



**Scheme 1.** Spontaneous photooxidation reaction of 11.

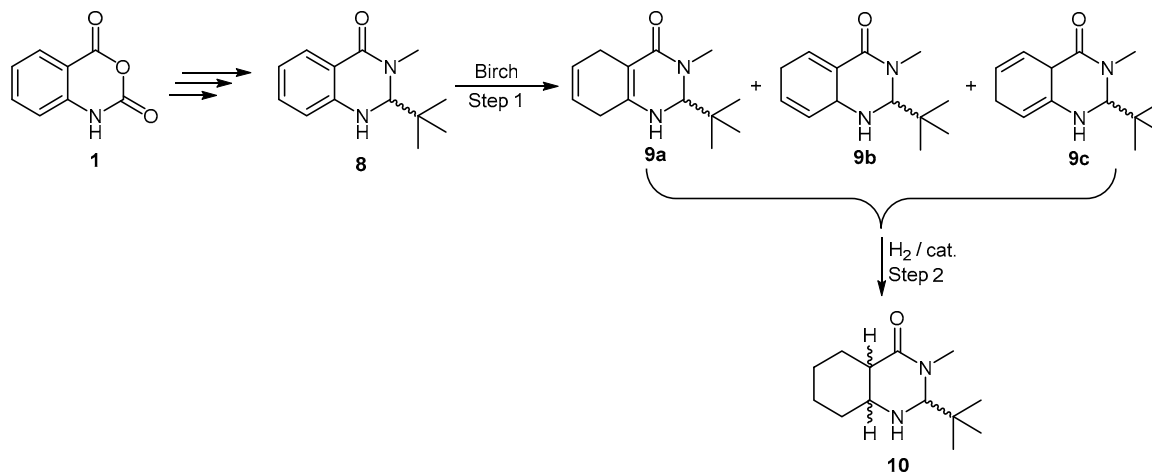
## 2. Results and Discussion

A recent topic of our research group has been the total reduction of the aromatic ring in 4-quinazolinone (1*H*)-one (**3**). Here, enantiomerically pure quinazolinone **3** was reduced diastereoselectively by hydrogenation with PtO<sub>2</sub> resulting in octahydroquinazolinone diastereomers **4**, **5**, and **6** in a ratio of 6:3:1. We found that the resulting *cis*-annulated derivatives **4** and **5** could be epimerized in the presence of KO*t*Bu, giving the corresponding *trans*-fused derivatives **6** and **7**, respectively, in good yields (Scheme 2) [16].



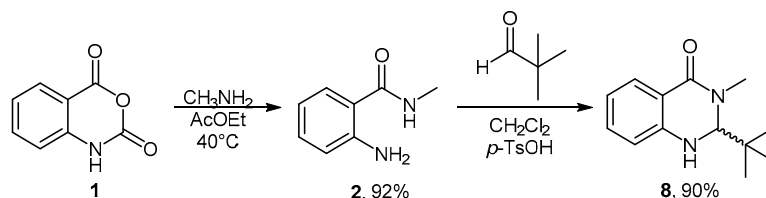
**Scheme 2.** Hydrogenation reaction of quinazolinone 3.

In the search for a new synthesis route with the same purpose as in **3**, quinazolinone **8** was proposed as a starting material and via Birch reduction [17], generating the possible intermediates **9a–c**. Afterwards, without purification, the catalytic hydrogenation of olefin [18] systems produce octahydroquinazolinone **10**, as shown in Scheme 3.



**Scheme 3.** Design of the total reduction of the aromatic ring of quinazolinone **8** in stages.

Previously, our research was focused on the preparation of the starting material (**8**) following the methodology reported in [19] where a reaction between isatoic anhydride **1** and methylamine in ethyl acetate at 40 °C results in the corresponding aminobenzamide **2** in 92% yield. In this work, instead, **8** is produced by the cyclocondensation of **2** with pivalaldehyde in dichloromethane and *p*-toluenesulfonic acid monohydrate with 90% yield (Scheme 4).



**Scheme 4.** Synthesis of quinazolinone (**8**).

The result is confirmed by a X-ray diffraction from suitable single-crystal where the *tert*-butyl group of quinazolinone (**8**) is shown to adopt a pseudo-axial conformation (Figure 1).

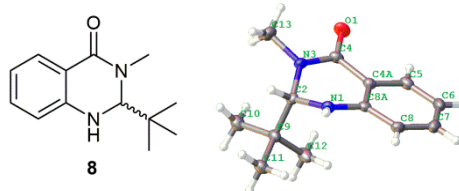
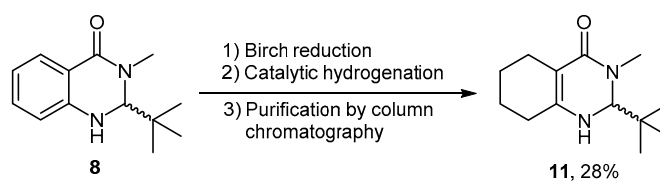


**Figure 1.** Structure and single-crystal X-ray diffraction of quinazolinone (**8**) showing the pseudo-axial conformation of *tert*-butyl group.

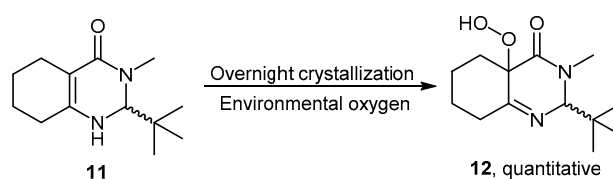
The Birch reduction of quinazolinone (**8**) was carried out (stage 1), without purification, and we proceeded with stage 2 (catalytic hydrogenation). When the product of step 2 was purified by column chromatography and characterized by <sup>1</sup>H-NMR, hexahydroquinazolinone (**11**) (yield 28%, Scheme 5) was obtained instead of **10**.



**Scheme 5.** Stepwise reduction of quinazolinone (**8**).

The <sup>1</sup>H-NMR spectrum of **11** shows a *tert*-butyl signal at 0.92 ppm, *N*-Me at 3.06 ppm, and C2 hydrogen at 4.2 ppm. The lack of an aromatic zone signals and two multiple signals between 1.41–1.74 and 2.04–2.27 ppm are of the new methylenes previously from the aromatic ring of **8**, which indicates that only partial reduction occurred.

Once the amorphous solid product **11** was characterized, it was recrystallized by diffusion overnight in *n*-hexane/CH<sub>2</sub>Cl<sub>2</sub> (80:20) solvent mixture (Scheme 6).



**Scheme 6.** Recrystallization by diffusion of **11** overnight.

Finally, after filtering, hexahydroquinazolinone (**12**) (Figure 2) was obtained whose structure was also confirmed by X-ray diffraction where a hydroperoxy group at the alpha position to the carbonyl group was noted.

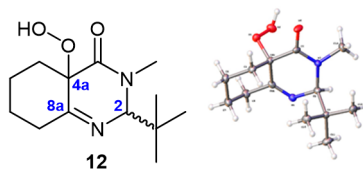


**Figure 2.** Structure and single-crystal X-ray diffraction of hexahydroquinazolinone (**12**). It should be noted that the hydroperoxy group is oriented to the opposite side as the *tert*-butyl group.

As expected, the orientation of the *tert*-butyl group in a pseudo-axial position in quinazolinone (**8**) (Figure 1) causes a significant steric effect and as a consequence, which forced the hydroperoxide group to attach to the opposite side, as observed in the X-ray structure of compound **12**.

The  $^1\text{H-NMR}$  spectrum of the compound **12** shows the *tert*-butyl signals at 0.98 ppm, *N*-Me at 3.05 ppm, the single signal for C2 hydrogen at 4.86 ppm, and aliphatic hydrogens between 1.55 and 2.89, respectively. In addition, from the characteristic signals of compound **12**, the  $^{13}\text{C-NMR}$  spectrum also shows the quaternary signals for C8a at 170.32 ppm and C4a at 76.32 ppm.

To confirm that the hydroperoxidized compound **12** was produced by a photooxidation reaction by exposure to ambient conditions, a kinetic study was carried out by means of  $^1\text{H-NMR}$  (Figure 3). Once compound **11** was purified, its  $^1\text{H-NMR}$  spectrum was immediately acquired ( $t_0 = 0$  h), and the characteristic signals of this product were noted. After 72 h ( $t_1$ ) and without opening the NMR tube, a spectrum was acquired again.

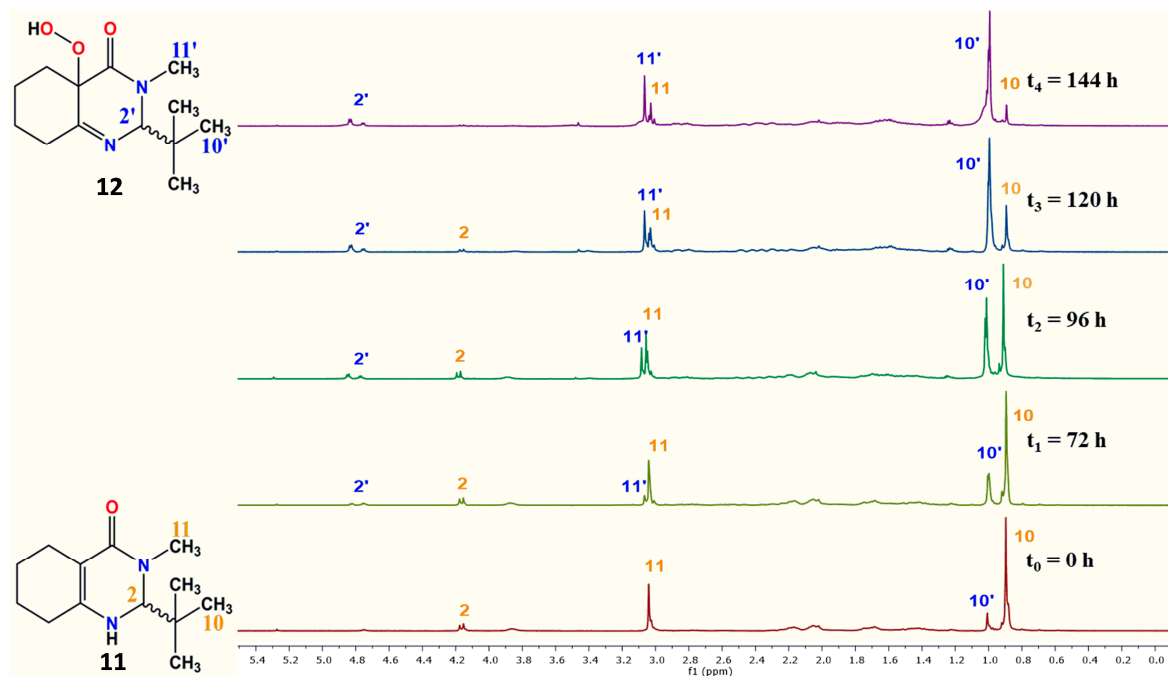


**Figure 3.** Kinetic study by  $^1\text{H-NMR}$  of environmental exposure of **11**.

It is interesting to observe that the signals at 1.00 ppm ( $10'$ ), 3.06 ppm ( $11'$ ), and 4.84 ppm ( $2'$ ) ppm at ( $t_1$ ) already increased, albeit only slightly. These signals eventually developed to be the corresponding hydrogens of **12** mentioned above. This is to show that even with the short span of light exposure before the first spectrum was obtained, the small amount of oxygen remained inside the NMR tube was enough to react with compound **11**.

Next, the NMR tube was exposed to the laboratory ambient conditions for three days with the spectrum obtained every 24 h ( $t_2 = 96$  h,  $t_3 = 120$  h, and  $t_4 = 144$  h). The spectrum of  $t_4$  shows that, by then, most of **11** was transformed into product **12**. It is important to comment that during the exposure time the volume of  $\text{CDCl}_3$  decreased, hence it was necessary to maintain a volume of 0.5 mL when spectra were taken.

It is also noted that, in  $^1\text{H-NMR}$  spectra, only signals corresponding to raw materials and products are observed, confirming the high yield and absence of competing mechanisms. This result demonstrates that the oxygen in the environment is responsible for the photooxidation reaction of compound **11** when it was recrystallized overnight.

To demonstrate that the absence of oxygen does not allow the hydroperoxidation reaction to occur, compound **11** was placed in a closed vial and after 72 h we observed only the original compound by TLC (from left, first spot with a  $R_f = 0.68$ , Figure 4). On the other hand, when **11** was placed in an open vial and covered with aluminum foil for 14 h, **12** was observed by TLC ( $R_f = 0.96$ , second spot). The third spot from the left (marked M) corresponds to a mixture of **11** and **12**, with the right spot, **12** as a reference.

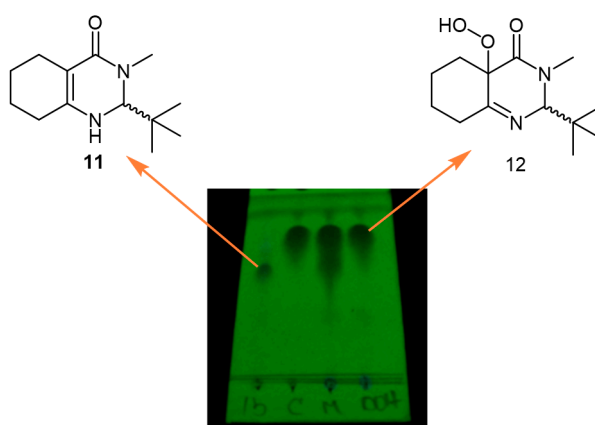


**Figure 4.** Thin layer chromatography (hexane:AcOEt, 6:4) for (1b) without oxygen, (C) with oxygen and covered with aluminum foil, (M) mixture of **11** and **12**, and (OOH) compound **12** for reference.

To confirm the role of light in the reaction, a control TLC experiment was also performed. Compound **11** was placed in a vial under a  $\text{N}_2$  atmosphere and covered with aluminum foil for 24 h which resulted in only **11** was observed with  $R_f = 0.35$  (Figure 5).

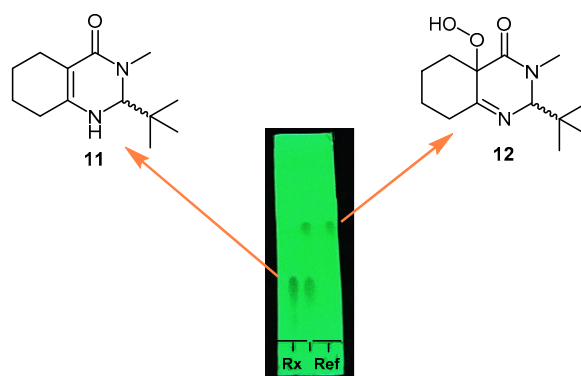


**Figure 5.** Thin layer chromatography (hexane:AcOEt, 8:2) of (Rx) in  $\text{N}_2$  atmosphere and without light; compound **12** for reference.

Furthermore, the reaction occurs very quickly, for even a short exposure to light and oxygen was sufficient to show traces of **12**, as can be seen in  $t_0$  in Figure 3. Finally, we found that with exposure to light for 6 h we were able to obtain the same result as overnight crystallization.

To confirm the importance of light exposure, it was necessary to make a detailed analysis of the kinetic study of Figure 3. Thus, Table 1 shows the  $^1\text{H-NMR}$  proportions of the raw material **11** and product **12**. Figure 6 illustrates the data in Table 1, where we can see that there is a sharp change in the rate of formation of **12** after 72 h where light was introduced to the vial.

**Table 1.** Proportions of compounds **11** and **12** by  $^1\text{H-NMR}$ .

$^1\text{H-NMR}$ Spectra	Exposure Time (h)	<b>11</b> (%)	<b>12</b> (%)	<b>12</b> (%)
1 <sup>a</sup>	0	87	13.0	
2 <sup>b</sup>	24	81	18.6	5.6
2 <sup>b</sup>	48	75	24.2	5.6
2 <sup>b</sup>	72	70	29.8	24.2
3	96	46	54.0	25
4	120	21	79.0	13
5	144	8	92	

<sup>a</sup> From sample preparation to its introduction into the NMR equipment. <sup>b</sup> The sample was a weekend within the NMR equipment.

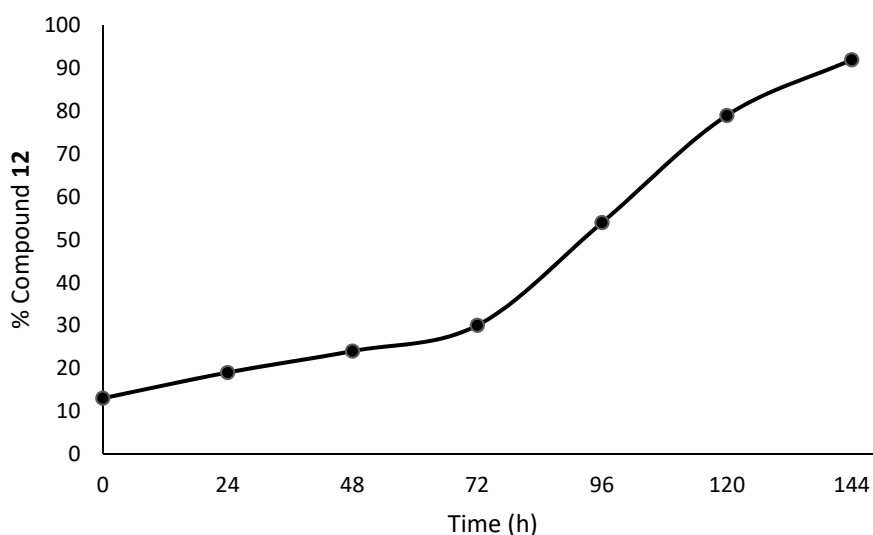
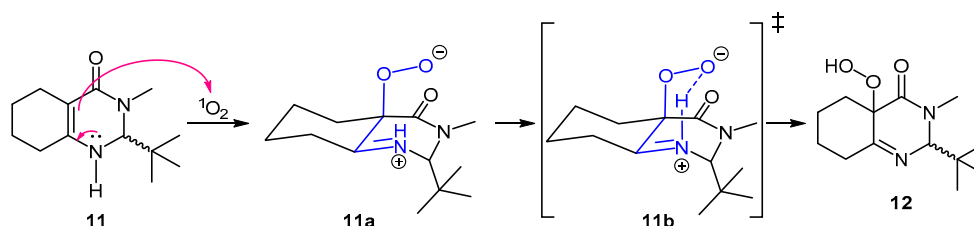


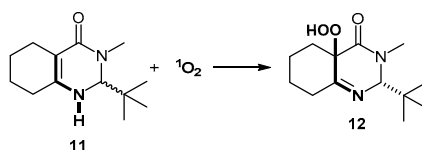
**Figure 6.** Proportion of **12** and time by  $^1\text{H-NMR}$ . Percentage of **12** was calculated relative to the signals of *tert*-butyl groups of **11** and **12**.

Based on the experimental evidence that has been shown, a possible reaction mechanism for the formation of hydroperoxidized **12** is proposed in Scheme 7.



**Scheme 7.** Proposed mechanism for the formation of product **12**.

We argue that hydroperoxidized **12** comes from the intermediate **11** through a Schenck reaction, also called an *ene* reaction, which additionally involves the singlet oxygen ( $^1\text{O}_2$ ) as a reactant (Scheme 8) [20,21].



**Scheme 8.** Spontaneous *ene* reaction of compound **11**.

In a previous study [22], we showed that, in the presence of light, photoinduced elimination of the *tert*-butyl group in quinazolinones achieved a high reactivity. This gives us motive to propose (Figure 7) that **11** could also absorb energy from light to give **11\*** and interact with oxygen from the environment ( $^3\text{O}_2$ ) to give rise to the formation of singlet oxygen ( $^1\text{O}_2$ ) through an energy transfer mechanism [23], which would result in a self-sensitizing process [24].

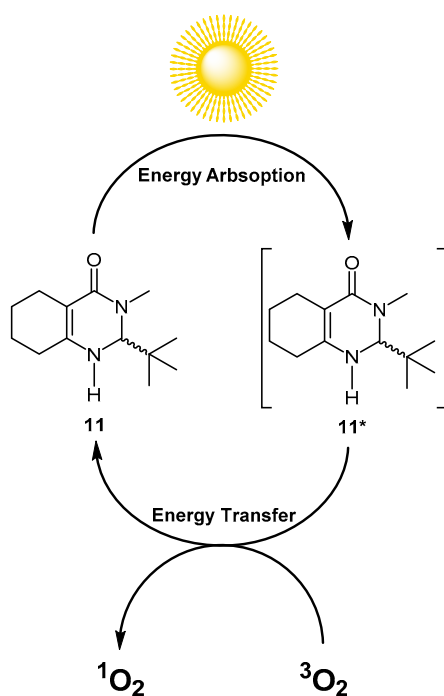
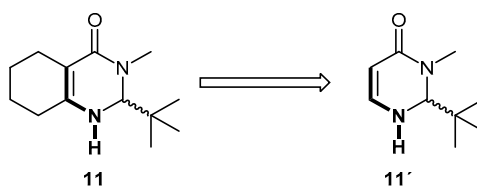


**Figure 7.** Formation of singlet oxygen ( $^1\text{O}_2$ ).

The general proposed pathway consists of two variants: A concerted or a stepwise mechanism [13]. The concerted pathway requires both a hydrogen atom at the allylic position and a favorable geometry in order to access the transition state kinetically [25]. Since the right-hand side ring has locked the amine hydrogen in its position, making it too rigid to be able to form a bond with the oxygen molecule, we eliminate this pathway.

For the stepwise mechanism, we explore probable intermediates following the theoretical and experimental study by Alberti and Orfanopoulos [13]. For our theoretical model, we have removed the cyclohexane ring from **11** to form **11'** (Scheme 9). The complete molecule **11** was used in a detailed study of orbital analysis, whereas model **11'** was used in order to reduce the computational cost in subsequent calculations of both locating the transition state and its confirmation by IRC.



**Scheme 9.** Proposed model molecule **11'**, which comes from **11**.

To validate the use of **11'**, as a preliminary study we performed an orbital analysis of both **11** and **11'** at the B3LYP/6-311++G\*\* level where we observed that **11'** shares a very similar HOMO and LUMO with **11**. This strongly suggests the use of **11'** in explore the second pathway. The product **12'** is defined in the same way.

As suggested by Alberti and Orfanopoulos [13], we consider the following intermediates: (a) biradical/dipolar, (b) perepoxide, and (c) 1,2-dioxetane (Figure 8).

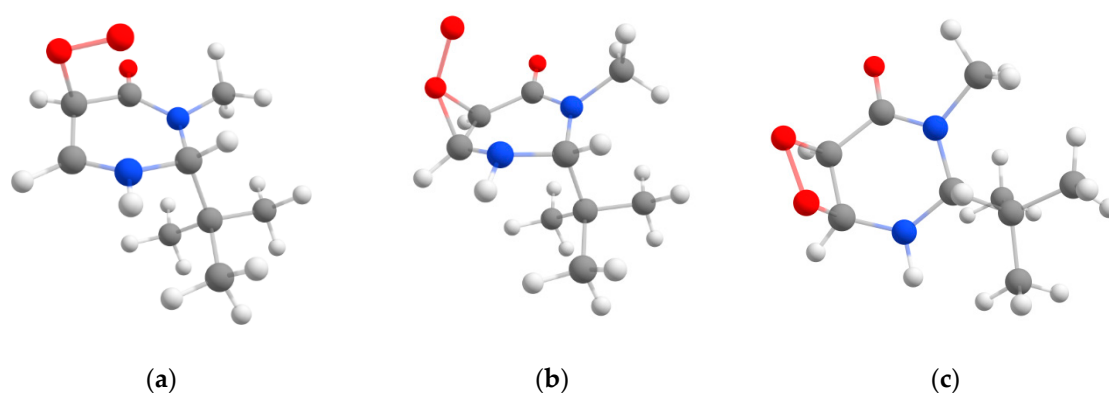


**Figure 8.** The proposed intermediates studied of the peroxidation reaction: (a) Biradical or zwitterion (dipolar), (b) perepoxide, and (c) 1,2-dioxetane.

Geometries of these intermediates were optimized at the same theoretical level which we found that only the Zwitterionic and the 1,2-dioxetane intermediates (labeled herein after as **I<sub>Z</sub>** and **I<sub>D</sub>** intermediates, respectively) were able to converge to stable structures whereas the perepoxide intermediate resulted in the partial dissociation of the oxygen molecule from **11'**.

In the next step, with the optimized structure of **11'** and  $^1\text{O}_2$  as reactant and **I<sub>Z</sub>** as product, the corresponding **TS1<sub>Z</sub>** were collocated by the QST2 method. This transition state is the result of a nucleophilic attack from the  $\alpha$ -carbon of the  $\alpha,\beta$ -unsaturated system to the electrophilic  $^1\text{O}_2$  (Figure 9a). The second transition state **TS1<sub>D</sub>**, from the same reaction of **11'** and  $^1\text{O}_2$  where **I<sub>D</sub>** is the product, shows the first oxygen... $\alpha$ -carbon bond (Figure 9b) while the nucleophilic attack from the second oxygen to the positive  $\beta$ -carbon to form the second bond strongly suggests a second intermediate.

Results from IRC calculations which connect a transition state to the correct reactant and product show that **TS1<sub>Z</sub>** leads to the intermediate **I<sub>Z</sub>** whereas **TS1<sub>D</sub>** did not lead to the reactants **11'** and  $^1\text{O}_2$  but to **I<sub>Z</sub>** instead. Combining the two results gives us a two-step mechanism: the first transition state leads to intermediate **I<sub>Z</sub>**. From there, a second transition state leads to the second intermediate **I<sub>D</sub>**.

In the next step, again we use the combination of QST2 and IRC methods to study the reactions between intermediates **I<sub>Z</sub>**, **I<sub>D</sub>** and the final product **12'**. For the formation of **12'** from intermediate **I<sub>Z</sub>** we found a six-member transition state **TS2<sub>Z</sub>** where a nucleophilic attack of the negatively charged oxygen to the partially positive hydrogen attached to the nitrogen atom **N1** is observed (Figure 10). IRC calculations were used to confirm the connection between this transition state to intermediate **I<sub>Z</sub>** and **12'**, respectively.

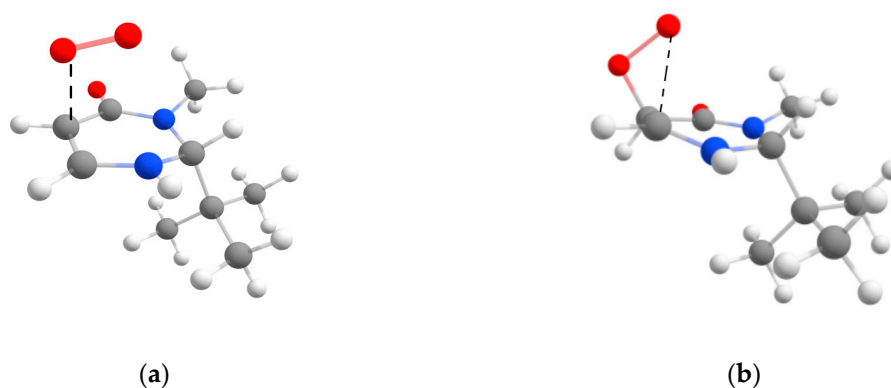


**Figure 9.** TS from QST2 calculation starting from the  $^1\text{O}_2$  and **11'** as reactants, and: (a) the dipolar intermediate, **TS1<sub>Z</sub>** ( $E = -687.577821$  Hartree) or (b) the 1,2-dioxetane, **TS1<sub>D</sub>** ( $E = -687.562242$  Hartree) as product.

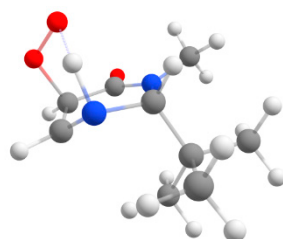


**Figure 10.** **TS2<sub>Z</sub>** from QST2 calculation starting from the **I<sub>Z</sub>** as reactant and the hydroperoxide as product **P** ( $E = -687.571828$  Hartree).

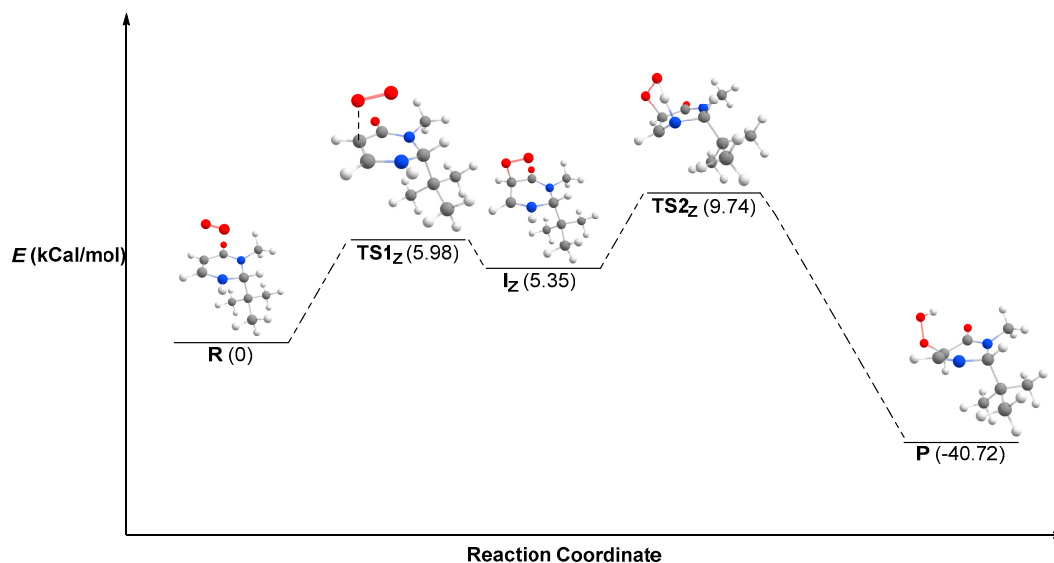
The transition state of the reaction between intermediate **I<sub>D</sub>** and **12'**, however, is the same as **TS1<sub>Z</sub>** since the hydrogen atom at the *N1* position, again due to its rigid conformation, cannot participate and, as a result, the reaction proceeds to the same **TS1<sub>Z</sub>** transition state.

Finally, taking into account all the hitherto theoretical and experimental evidence, we propose the following mechanism for the transformation of **11** to **12**. In the first step, the singlet oxygen molecule approaches **11** from the opposite site of the *tert*-Bu substituent, then a nucleophilic attack to the  $\alpha$ -carbon results in an unstable dipolar/zwitterion intermediate **I<sub>Z</sub>** via the transition state **TS1<sub>Z</sub>**. The X-ray diffraction structure (Figure 2) gives evidence supporting this step. In the second step, another intermolecular nucleophilic attack from the remaining free oxygen of the peroxide to the positively-charged hydrogen (at *N1*) via the second transition state **TS2<sub>Z</sub>** that leads to the final product **12** (Scheme 10).

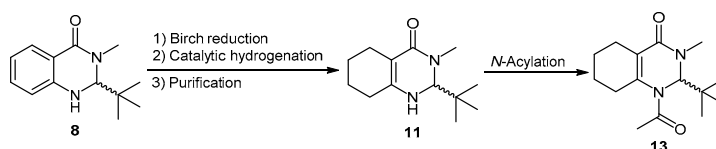
To further confirm the proposed mechanism, in which the hydrogen atom plays a crucial role, an acetylation at *N1* by means of a Birch reduction and catalytic hydrogenation were carried out in quinazolinone **8**. Subsequently, purification of compound **11** *N*-acylation was performed, obtaining compound **13** (Scheme 11).

Product **13** was then crystallized in the same way as for compound **11** (Scheme 12). Subsequently, the crystals was obtained and analyzed by  $^1\text{H}$  and  $^{13}\text{C}$  NMR, and it was confirmed that photooxidation did not occur. In the  $^1\text{H}$ -NMR spectrum, signals of *tert*-butyl are observed at 0.89 ppm, *N*-Me at 2.13 ppm, and a protecting group of hydrogens remains at 3.03 ppm. On the other hand, in the  $^{13}\text{C}$ -NMR spectrum, four quaternary carbons are observed: two carbonyls at 163.5 and 170.8 ppm, *C4a* at 122.3 ppm, and *C8a* 140.9 ppm.

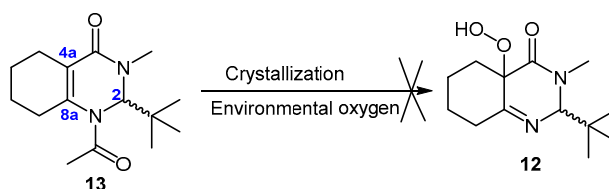
The single crystals obtained from compound **13** were diffracted; again, the X-ray structure shows a pseudo-axial position of the *tert*-butyl group in the acquired structure (Figure 11).



**Scheme 10.** Reaction coordinate which describes the most probable reaction mechanism of the formation of **12** from **11**.



**Scheme 11.** Synthesis of **13**.



**Scheme 12.** Overnight crystallization of **13**.

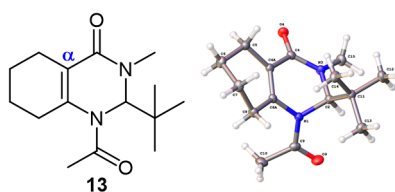
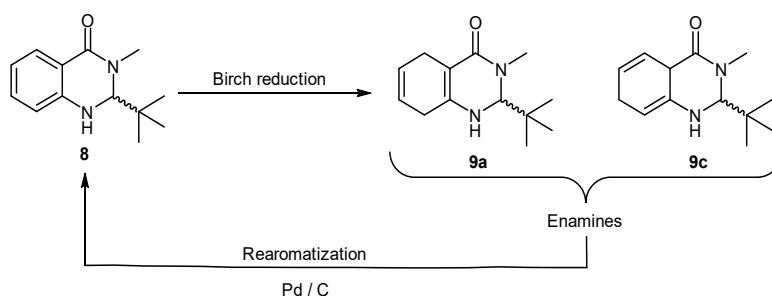


**Figure 11.** Structure and X-ray diffraction of hexahydroquinazolinone (**13**).

We have shown that by exchanging allylic hydrogen in *N*1, the photooxidation of compound **13** does not occur under crystallization by diffusion. We suggest that the stability of hexahydroquinazolinone (**13**) increases and as a result the pair of electrons is not available to promote the nucleophilic attack of the  $C\alpha$  on singlet oxygen (Scheme 7).

$^1\text{H-NMR}$  evidence shows that the photooxidation reaction of **11** occurs in good yield. However, the corresponding yield of the precursor **11** was rather low. It has been reported [26–30] that endocyclic enamines can be rearomatized in the presence of catalysts, such as Pd/C, PdCl<sub>2</sub>, PdBr<sub>2</sub>, Pd(COD)<sub>2</sub>, Pd(OAc)<sub>2</sub>, or Pd(TFA)<sub>2</sub>. We note the enamine moiety of **11** (Scheme 1, purple box), which has been described as a possible product of the Birch reaction (step 1, Scheme 3). The same observation

applies to **9a** or **9c**. These observations strongly suggest that the presence of Pd/C would accelerate the rearomatization process when catalytic hydrogenation takes place (Scheme 13). This would explain the low yields mentioned above.



**Scheme 13.** Rearomatization of hexahydroquinazolinones (**9a** or **9c**).

### 3. Materials and Methods

Dichloromethane, ethyl acetate, and hexane were distilled before use. Toluene, acetonitrile, *tert*-butanol, isatoic anhydride, methylamine, *p*-toluene sulfonic acid, pivalaldehyde, sodium bicarbonate, sodium sulfate, sodium, palladium/carbon, 4,4-dimethylamino pyridine, and acetyl chloride were acquired from Sigma-Aldrich (St. Louis, MI, USA) and used without further purification. Reactions were monitored by thin layer chromatography (TLC) on Al plates coated with silica gel with fluorescent indicator 60 F254 (Merck-Mexico, Mexico City, Mexico). Column chromatography was performed on silica gel 60 (0.040–0.063 mm, Merck-Mexico, Mexico City, Mexico).

#### 3.1. Analytical Methods

NMR spectra of products as well as the proportions of each product in the reaction mixture were recorded on Varian Gemini at 200 MHz and Varian Mercury 400 MHz ( $^1\text{H-NMR}$ ), and 50 and 100 MHz ( $^{13}\text{C-NMR}$ ) spectrometers, using  $\text{CDCl}_3$  as a solvent and tetramethylsilane (TMS) as an internal standard. A mass spectrometric analysis was performed using an Agilent 6530 quadrupole time-of-flight (QTOF) LCMS with an electrospray ionization (ESI) source (Agilent Technologies, Santa Clara, CA, USA). A mass spectrometry analysis was conducted in positive ion mode, set for a detection of mass-to-charge ratio ( $m/z$ ) of 100–1000. The X-ray structures were obtained using an APEX-Bruker apparatus.

#### 3.2. Theoretical Study

All calculations were carried out using the Gaussian 09 suite of programs [31]. Geometry optimizations were carried out at the B3LYP/6-311++G\*\* level of theory [32–36] followed by characterization by frequency calculations at the same level of the theory, in which zero-point energy corrections (ZPE) and thermal corrections at the standard state (298.15 K and 1 atm) were obtained.

Initial geometry for the model molecule **11'** was constructed from the optimized geometry of **11** by substituting the cyclohexyl moiety by suitable hydrogen atoms. Similar methodology was applied in order to obtain the geometric parameters for the product, which has taken advantage of X-ray parameters from the obtained structure. The intermediates, such as peroxide and biradical/dipolar, were constructed from the optimized geometry of **11'** placing the  $\text{O}_2$  residue into the *endo* position and then optimized at the same level of theory. In order to obtain the initial coordinates for the transition state, QST2 [37] calculations were performed starting from the product and reactants' optimized geometries. The resulting transition states were confirmed by frequency calculation. An intrinsic reaction coordinate (IRC) calculation [38] was performed at the same level of theory in order to verify that the TS structure connects with the reactant and product. Coordinates for selected structures and thermochemistry data are given in the Supplementary Material.

### 3.3. Chemistry

#### 3.3.1. Synthesis of 2-(*tert*-butyl)-3-methyl-2,3-dihydroquinazolin-4(1H)-one (**8**)

Quinazolinone (**8**) was prepared according to a known procedure [19] from isatoic anhydride (6 g, 30.68 mmol), methylamine in isobutanol (18.2 mL, 122.7 mmol), and ethyl acetate (50 mL). The resulting material was filtered and concentrated in a rotavapor. The crude mixture (2.06 g), *p*-toluenesulfonic acid (0.10 g, 5% *w/w*), pivalaldehyde (1.86 mL, 1.2 equiv.), and dichloromethane (60 mL) was refluxed for 5 h and the resulting material was filtered and evaporated under reduced pressure, purified over SiO<sub>2</sub> using hexane-ethyl acetate (9:1 to 6:4). Its structure was confirmed by <sup>1</sup>H and <sup>13</sup>C-NMR, and compared with available information in the literature [18]. Yield: 2.71 g, 90%; white solid, mp: 145–146 °C. <sup>1</sup>H NMR (200 MHz, CDCl<sub>3</sub>): δ 0.80 (s, 9H), 2.28 (s, 3H), 5.88 (s, 1H), 7.14–7.32 (m, 1H), 7.36 (dd, *J* = 7.6, 1.2 Hz, 1H), 7.55 (td, *J* = 7.7, 1.6 Hz, 1H), 7.67 (s, 1H), 8.02 (dd, *J* = 7.7, 1.7 Hz, 1H). <sup>13</sup>C NMR (CDCl<sub>3</sub>, 50 MHz): δ 26.3, 38.5, 41.9, 79.9, 113.1, 116.6, 118.1, 128.1, 133.4, 146.5, 163.8. HREIMS *m/z* 218.1440 (calculated for C<sub>13</sub>H<sub>18</sub>N<sub>2</sub>O, 218.1419). Crystallographic data is deposited at Cambridge Crystallographic Data Center: CCDC no. 2006915.

#### 3.3.2. Synthesis of 2-(*tert*-butyl)-3-methyl-2,3,5,6,7,8-hexahydroquinazolin-4(1H)-one (**11**)

Ammonia (50 mL) was condensed to −78 °C before the slow addition of 1.0 g (4.6 mmol) of 2-(*tert*-butyl)-3-methyl-2,3-dihydroquinazolin-4(1H)-one (**8**), and sodium (0.64 g, 28 mmol). The resulting solution was stirred for 30 min and then treated with 1.4 mL (14 mmol) of *tert*-butanol. The reaction mixture was stirred at this temperature for 1 h. The reaction was quenched adding ammonium chloride (0.64 g, 18.5 mmol). Ammonia was evaporated at ambient temperature and reaction crude was dissolved in dichloromethane, dried with Na<sub>2</sub>SO<sub>4</sub> and the excess solvent was evaporated under reduced pressure. A suspension of reaction crude (0.8 g), Pd/C (0.04 g, 5% *w/w*), and methanol (60 mL) was placed in a 100 mL flask containing a stir bar, then the system was closed with a septum. Two balloons were placed with hydrogen and the reaction was stirred overnight. The reaction mixture was filtered and concentrated in a rotavapor, then purified by column chromatography on silica, eluting with hexane-ethyl acetate (9:1 to 2:8). Yield: 130 mg, 28%; light-yellow solid; mp: 134–137 °C. <sup>1</sup>H NMR (200 MHz, CDCl<sub>3</sub>) δ 4.18 (d, 1H, *J* = 4.6 Hz, 1H), 3.88 (s, 1H), 3.06 (s, 3H), 2.27–2.04 (m, 4H), 1.77–1.36 (m, 4H), 0.91 (s, 9H). <sup>13</sup>C NMR of this compound was acquired for 72 h, however many signals were observed due to the high reactivity of **11**.

#### 3.3.3. Synthesis of 2-(*tert*-Butyl)-4a-hydroperoxy-3-methyl-2,4a,5,6,7,8-hexahydroquinazolin-4(3H)-one (**12**)

Hexahydroquinazolin-4(1H)-one **11** (0.071 g, 0.32 mmol) was dissolved in 2 mL dichloromethane inside a suitable test tube, then 8 mL of hexane was added carefully, the system was closed with a cotton septum and left exposed to the environment overnight. Compound **12** was thus isolated as a white crystal. Yield: 81 mg (quantitative); mp: 152–154 °C; <sup>1</sup>H NMR (500 MHz, CDCl<sub>3</sub>) δ 1.02 (s, 9H), 1.55–1.67 (m, 3H), 1.94–1.97 (m, 1H), 2.08–2.11 (m, 1H), 2.39–2.47 (m, 2H), 2.94–2.95 (m, 1H) 3.10 (s, 3H), 4.90 (s, 1H). <sup>13</sup>C NMR (125 MHz, CDCl<sub>3</sub>) δ 170.3, 168.6, 85.3, 76.3, 40.1, 37.0, 34.2, 33.7, 28.5, 27.2, 20.5. HREIMS *m/z* 254.1654 (calculated for C<sub>13</sub>H<sub>22</sub>N<sub>2</sub>O<sub>3</sub>, 254.1630). Crystallographic data is deposited at Cambridge Crystallographic Data Center: CCDC no. 2006916.

#### 3.3.4. Synthesis of 1-Acetyl-2-(*tert*-butyl)-3-methyl-2,3,5,6,7,8-hexahydroquinazolin-4(1H)-one (**13**)

Hexahydroquinazolin-4(1H)-one (**11**) (0.8 g, 3.6 mmol), 4-dimethylaminopyridine (0.43 g, 3.6 mmol) and toluene/acetonitrile solution 9:1 (40 mL) was added to a 100 mL flask. It was placed in an ice bath and the system purged with nitrogen. Acetyl chloride (0.3 mL, 4.3 mmol) was added dropwise and the reaction was stirred overnight. The reaction crude was filtered, evaporated, and purified by column chromatography on silica, eluting with hexane-ethyl acetate (9:1 to 3:7). Yield: quantitative; white solid; mp: 146–148 °C; <sup>1</sup>H NMR (200 MHz, CDCl<sub>3</sub>) δ 5.44 (s, 1H), 3.03 (s, 3H), 2.79–2.54 (m, 2H), 2.13 (s, 3H),

2.09–1.98 (m, 2H), 1.91–1.36 (m, 4H), 0.89 (s, 9H).  $^{13}\text{C}$  NMR (50 MHz  $\text{CDCl}_3$ )  $\delta$  170.8, 163.5, 122.3, 38.4, 37.1, 30.5, 27.1, 27.0, 24.1, 22.6, 22.5, 21.6. HREIMS  $m/z$  264.1843 (calculated for  $\text{C}_{15}\text{H}_{24}\text{N}_2\text{O}_2$ , 264.1838). Crystallographic data is deposited at Cambridge Crystallographic Data Center CCDC: no. 2007030.

#### 4. Conclusions

We have shown that the photooxidation reaction of compound **11** occurs in the absence of sensitizers and only with exposure to ambient air.  $^1\text{H}$ -NMR kinetics evidence also shows that it is a process with very reasonable yield. The presence of allylic hydrogen in  $N$ -H bond plays an important role in the mechanism which facilitates the nucleophilic attack of  $\alpha$ -C by singlet oxygen, and in the formation of the six-member cyclical transition state. The low yield of compound **11** could be explained by the aromatization reaction of enamines in the presence of Pd/C. Theoretical study supports a stepwise mechanism for the *ene* reaction between **11** and  $^1\text{O}_2$ . The two-step reaction proceeds via a dipolar intermediate in which the first TS corresponds to the nucleophilic attack of the  $\alpha$ -carbon to the  $^1\text{O}_2$  yielding the dipolar intermediate. The second step involves a nucleophilic attack from the negative oxygen to the partial positive hydrogen leading to the final product **12**. Applications of this methodology to other related 4-quinazolinone derivatives are currently being carried out in our laboratory.

**Supplementary Materials:** The following are available online, Figure S1:  $^1\text{H}$  spectrum (200 MHz,  $\text{CDCl}_3$ ) of **8**, Figure S2:  $^{13}\text{C}$  spectrum (100 MHz,  $\text{CDCl}_3$ ) of **8**, Figure S3:  $^1\text{H}$  spectrum (200 MHz,  $\text{CDCl}_3$ ) of **11**, Figure S4:  $^{13}\text{C}$  spectrum (50 MHz,  $\text{CDCl}_3$ ) of **11**, Figure S5:  $^1\text{H}$  spectrum (500 MHz,  $\text{CDCl}_3$ ) of **12**, Figure S6:  $^{13}\text{C}$  spectrum (125 MHz,  $\text{CDCl}_3$ ) of **12**, Figure S7:  $^1\text{H}$  spectrum (200 MHz,  $\text{CDCl}_3$ ) of **13**, Figure S8:  $^{13}\text{C}$  spectrum (50 MHz,  $\text{CDCl}_3$ ) of **13**, Figure S9: Cartesian coordinates from optimized structure of **11** at the B3LYP/6-311++G\*\* level of theory, Figure S10: Cartesian coordinates from optimized structure of **12** at the B3LYP/6-311++G\*\* level of theory, Figure S11: Cartesian coordinates from optimized structure of the **R** at the B3LYP/6-311++G\*\* level of theory, Figure S12: Cartesian coordinates from optimized structure of the **P** at the B3LYP/6-311++G\*\* level of theory, Figure S13: Cartesian coordinates from optimized structure of the **TS1z** at the B3LYP/6-311++G\*\* level of theory, Figure S14: Cartesian coordinates from optimized structure of the **TS1D** at the B3LYP/6-311++G\*\* level of theory, Figure S15: Cartesian coordinates from optimized structure of the **TS2z** at the B3LYP/6-311++G\*\* level of theory, Figure S16: Cartesian coordinates from optimized structure of the **TS2D** at the B3LYP/6-311++G\*\* level of theory, Figure S17: Cartesian coordinates from optimized structure of the **Iz** at the B3LYP/6-311++G\*\* level of theory, Figure S18: Cartesian coordinates from optimized structure of the **Id** at the B3LYP/6-311++G\*\* level of theory, Table S1: Crystal data and structure refinement for 135leo (2-(*tert*-butyl)-3-methyl-2,3-dihydroquinazolin-4(1H)-one (**8**)), Table S2: Crystal data and structure refinement for leo144a (2-(*tert*-butyl)-4a-hydroperoxy-3-methyl-2,4a,5,6,7,8-hexahydroquinazolin-4(3H)-one (**12**)), Table S3: Crystal data and structure refinement for redn (1-acetyl-2-(*tert*-butyl)-3-methyl-2,3,5,6,7,8-hexahydroquinazolin-4(1H)-one (**13**)), Table S4: Bond Lengths for 135leo (2-(*tert*-butyl)-3-methyl-2,3-dihydroquinazolin-4(1H)-one (**8**)), Table S5: Bond Angles for 135leo (2-(*tert*-butyl)-3-methyl-2,3-dihydroquinazolin-4(1H)-one (**8**)), Table S6 Hydrogen Atom Coordinates ( $\text{\AA}\times 104$ ) and Isotropic Displacement Parameters ( $\text{\AA}^2\times 103$ ) for 135leo (2-(*tert*-butyl)-3-methyl-2,3-dihydroquinazolin-4(1H)-one (**8**)), Table S7: Crystal data and structure refinement for leo144a (2-(*tert*-butyl)-4a-hydroperoxy-3-methyl-2,4a,5,6,7,8-hexahydroquinazolin-4(3H)-one (**12**)), Table S8: Fractional Atomic Coordinates ( $\times 104$ ) and Equivalent Isotropic Displacement Parameters ( $\text{\AA}^2\times 103$ ) for leo144a (2-(*tert*-butyl)-4a-hydroperoxy-3-methyl-2,4a,5,6,7,8-hexahydroquinazolin-4(3H)-one (**12**)) Ueq is defined as 1/3 of the trace of the orthogonalised UIJ tensor, Table S9: Anisotropic Displacement Parameters ( $\text{\AA}^2\times 103$ ) for leo144a (2-(*tert*-butyl)-4a-hydroperoxy-3-methyl-2,4a,5,6,7,8-hexahydroquinazolin-4(3H)-one (**12**)). The Anisotropic displacement factor exponent takes the form:  $-2\pi^2[h_2a^*2U_{11}+2h_1ka^*b^*U_{12}+\dots]$ , Table S10: Bond Lengths for leo144a (2-(*tert*-butyl)-4a-hydroperoxy-3-methyl-2,4a,5,6,7,8-hexahydroquinazolin-4(3H)-one (**12**)), Table S11: Bond Angles for leo144a (2-(*tert*-butyl)-4a-hydroperoxy-3-methyl-2,4a,5,6,7,8-hexahydroquinazolin-4(3H)-one (**12**)), Table S12: Torsion Angles for leo144a (2-(*tert*-butyl)-4a-hydroperoxy-3-methyl-2,4a,5,6,7,8-hexahydroquinazolin-4(3H)-one (**12**)), Table S13: Hydrogen Atom Coordinates ( $\text{\AA}\times 104$ ) and Isotropic Displacement Parameters ( $\text{\AA}^2\times 103$ ) for leo144a (2-(*tert*-butyl)-4a-hydroperoxy-3-methyl-2,4a,5,6,7,8-hexahydroquinazolin-4(3H)-one (**12**)), Table S14: Crystal data and structure refinement for redn (1-acetyl-2-(*tert*-butyl)-3-methyl-2,3,5,6,7,8-hexahydroquinazolin-4(1H)-one (**13**)), Table S15: Fractional Atomic Coordinates ( $\times 104$ ) and Equivalent Isotropic Displacement Parameters ( $\text{\AA}^2\times 103$ ) for redn (1-acetyl-2-(*tert*-butyl)-3-methyl-2,3,5,6,7,8-hexahydroquinazolin-4(1H)-one (**13**)). Ueq is defined as 1/3 of the trace of the orthogonalised UIJ tensor, Table S16: Anisotropic Displacement Parameters ( $\text{\AA}^2\times 103$ ) for redn (1-acetyl-2-(*tert*-butyl)-3-methyl-2,3,5,6,7,8-hexahydroquinazolin-4(1H)-one (**13**)). The Anisotropic displacement factor exponent takes the form:  $-2\pi^2[h_2a^*2U_{11}+2h_1ka^*b^*U_{12}+\dots]$ , Table S17: Bond Lengths for redn (1-acetyl-2-(*tert*-butyl)-3-methyl-2,3,5,6,7,8-hexahydroquinazolin-4(1H)-one (**13**)),

Table S18: Bond Angles for redn (1-acetyl-2-(tert-butyl)-3-methyl-2,3,5,6,7,8-hexahydroquinazolin-4(1H)-one (13), Table S19: Hydrogen Atom Coordinates ( $\text{\AA}\times 10^4$ ) and Isotropic Displacement Parameters ( $\text{\AA}^2\times 10^3$ ) for redn (1-acetyl-2-(tert-butyl)-3-methyl-2,3,5,6,7,8-hexahydroquinazolin-4(1H)-one (13).

**Author Contributions:** A.M., J.R.V.-C., and J.E. conceived and designed the experiments; J.E. wrote the paper. All authors have read and agreed to the published version of the manuscript.

**Funding:** This research received no external funding.

**Acknowledgments:** We would like to thank CONACyT for financial support (project no. CB2015/256653). Adrian Méndez gratefully acknowledges CONACyT for a scholarship (573014).

**Conflicts of Interest:** The authors declare no conflict of interest.

## References

1. Baklanov, A.V.; Parker, D.H. Weakly Bound Environment of Molecular Oxygen as a Catalyst of Photooxidation. *Kinet. Catal.* **2020**, *61*, 174–197. [[CrossRef](#)]
2. Taniguchi, T. Strategy for the Use of Molecular Oxygen in Organic Synthesis. *Synlett* **2020**, *31*. [[CrossRef](#)]
3. Bian, C.; Singh, A.K.; Niu, L.; Yi, H.; Lei, A. Visible-Light-Mediated Oxygenation Reactions using Molecular Oxygen. *Asian J. Org. Chem.* **2017**, *6*, 386–396. [[CrossRef](#)]
4. Xie, X.; Zhang, Z.; Hu, Y.; Cheng, H. A mechanistic kinetic model for singlet oxygen mediated self-sensitized photo-oxidation of organic pollutants in water. *Chem. Eng. J.* **2018**, *334*, 1242–1251. [[CrossRef](#)]
5. Rontani, J.F.; Belt, S.T. Photo- and autoxidation of unsaturated algal lipids in the marine environment: An overview of processes, their potential tracers, and limitations. *Org. Geochem.* **2020**, *139*, 103941. [[CrossRef](#)]
6. Davies, M.J. Singlet oxygen-mediated damage to proteins and its consequences. *Biochem. Biophys. Res. Commun.* **2003**, *305*, 761–770. [[CrossRef](#)]
7. Srivastava, V.; Singh, P.K.; Singh, P.P. Eosin Y catalysed visible-light mediated aerobic oxidation of tertiary amines. *Tetrahedron Lett.* **2019**, *60*, 151041. [[CrossRef](#)]
8. Zhang, M.; Lan, H.; Li, N.; Zhong, Q.; Zhu, H.; Liu, C.; Zhao, H.W. Photocatalyst-Free Singlet Oxygen-Induced Oxygenation: A Strategy for the Preparation of 5-Cyano-2-Pyridones Driven by Blue-Light Irradiation. *J. Org. Chem.* **2020**, *85*, 8279–8286. [[CrossRef](#)]
9. Griesbeck, A.G.; Cho, M. Singlet oxygen addition to homoallylic substrates in solution and microemulsion: Novel secondary reactions. *Tetrahedron Lett.* **2009**, *50*, 121–123. [[CrossRef](#)]
10. Zhang, Y.; Schilling, W.; Das, S. Metal-Free Photocatalysts for C-H Bond Oxygenation Reactions with Oxygen as the Oxidant. *ChemSusChem* **2019**, *12*, 2898–2910. [[CrossRef](#)]
11. Fukuzumi, S.; Lee, Y.M.; Nam, W. Photocatalytic oxygenation reactions using water and dioxygen. *ChemSusChem* **2019**, *12*, 3931–3940. [[CrossRef](#)] [[PubMed](#)]
12. He, J.; Hu, J.; Mo, X.; Hao, Q.; Fan, Z.; He, G.; He, Q. Novel photocatalyst nitrogen-doped simonkolleite  $\text{Zn}_5(\text{OH})_8\text{Cl}_2\cdot\text{H}_2\text{O}$  with vis-up-conversion photoluminescence and effective visible-light photocatalysis. *Appl. Phys. A* **2019**, *125*, 3. [[CrossRef](#)]
13. Alberti, M.N.; Orfanopoulos, M. Unraveling the mechanism of the singlet oxygen ene reaction: Recent computational and experimental approaches. *Chem. Eur. J.* **2010**, *16*, 9414–9421. [[CrossRef](#)]
14. Lanteri, D.; Quattrosoldi, S.; Soccio, M.; Basso, A.; Cavallo, D.; Munari, A.; Riva, R.; Lotti, N.; Moni, L. Regioselective photooxidation of citronellol: A way to monomers for functionalized bio-polyesters. *Front. Chem.* **2020**, *8*, 85. [[CrossRef](#)] [[PubMed](#)]
15. Ghogare, A.A.; Greer, A. Using singlet oxygen to synthesize natural products and drugs. *Chem. Rev.* **2016**, *116*, 9994–10034. [[CrossRef](#)] [[PubMed](#)]
16. Priego, J.; Flores, P.; Ortiz-Nava, C.; Escalante, J. Synthesis of enantiopure cis- and trans-2-aminocyclohexane-1-carboxylic acids from octahydroquinazolin-4-ones. *Tetrahedron Asymmetry* **2004**, *15*, 3545–3549. [[CrossRef](#)]
17. Zimmerman, H.E. A mechanistic analysis of the Birch reduction. *Acc. Chem. Res.* **2012**, *45*, 164–170. [[CrossRef](#)]
18. Méndez-Ochoa, A. Síntesis y Resolución de 4-Quinazolinonas y su Posible Utilidad en la Síntesis de Ácidos  $\beta$ -Aminociclohexancarboxílicos. Master's Thesis, Autonomous Morelos State University, Morelos, Mexico, 2017.

19. Escalante, J.; Ortíz-Nava, C.; Flores, P.; Priego, J.M.; García-Martínez, C. Synthesis, NMR and crystallographic studies of 2-substituted dihydroquinazolinones derived from (S)-phenylethylamine. *Molecules* **2007**, *12*, 173–182. [[CrossRef](#)]
20. Schenck, G.O. Understanding and Manipulating Excited-State Processes. German Patent DE-B 933925, 6 October 1955.
21. Schenck, G.O.; Eggert, H.; Denk, W. Photochemische Reaktionen III. Über die Bildung von Hydroperoxyden bei photosensibilisierten Reaktionen von O<sub>2</sub> mit geeigneten Akzeptoren, insbesondere mit  $\alpha$ - und  $\beta$ -Pinen. *Liebigs Ann. Chem.* **1953**, *584*, 177. [[CrossRef](#)]
22. Cabrera-Rivera, F.A.; Ortíz-Nava, C.; Escalante, J.; Hernández-Pérez, J.M.; Hô, M. Photoinduced elimination in 2,3-dihydro-2-*tert*-butyl-3-benzyl-4 (1H)-quinazolinone: Theoretical calculations and radical trapping using TEMPO derivatives. *Synlett* **2012**, *23*, 1057–1063.
23. Aganda, K.C.C.; Hong, B.; Lee, A. Aerobic  $\alpha$ -Oxidation of N-Substituted Tetrahydroisoquinolines to Dihydroisoquinolones via Organo-photocatalysis. *Adv. Synth. Catal.* **2019**, *5*, 1124–1129. [[CrossRef](#)]
24. Manju, T.; Manoj, N.; Braun, A.M.; Oliveros, E. Self-sensitized photooxidation of N-methyl phenothiazine: Acidity control of the competition between electron and energy transfer mechanisms. *Photochem. Photobiol. Sci.* **2012**, *11*, 1744–1755. [[CrossRef](#)]
25. Davies, A.G.; Schiesser, C.H. A PM3 study of the reactions of propene with singlet oxygen and other enophiles. *Tetrahedron* **1991**, *47*, 1707–1726. [[CrossRef](#)]
26. Cossy, J.; Belotti, D. Aromatization of enamines promoted by a catalytic amount of Pd/C. Synthesis of aromatic Amines. *Org. Lett.* **2002**, *4*, 2557–2559. [[CrossRef](#)]
27. Chen, Z.; Zeng, H.; Girard, S.A.; Wang, F.; Chen, N.; Li, C.J. Formal direct cross-coupling of phenols with amines. *Angew. Chem. Int. Ed.* **2015**, *54*, 14487–14491. [[CrossRef](#)]
28. Qiu, Z.; Li, J.-S.; Li, C.-J. Formal aromaticity transfer for palladium-catalyzed coupling between phenols and pyrrolidines/indolines. *Chem. Sci.* **2017**, *8*, 6954–6958.
29. Chen, S.; Liao, Y.; Zhao, F.; Qi, H.; Liu, S.; Deng, G.J. Palladium-catalyzed direct arylation of indoles with cyclohexanones. *Org. Lett.* **2014**, *16*, 1618–1621. [[CrossRef](#)]
30. Jumde, V.R.; Petricci, E.; Petrucci, C.; Santillo, N.; Taddei, M.; Vaccaro, L. Domino hydrogenation–reductive amination of phenols, a simple process to access substituted cyclohexylamines. *Org. Lett.* **2015**, *17*, 3990–3993.
31. Frisch, M.J.; Trucks, G.W.; Schlegel, H.B.; Scuseria, G.E.; Robb, M.A.; Cheeseman, J.R.; Scalmani, G.; Barone, V.; Petersson, G.A.; Nakatsuji, H.; et al. *Gaussian 09*; Revision, A.02; Gaussian, Inc.: Wallingford, CT, USA, 2016.
32. Becke, A.D. Density-functional exchange-energy approximation with correct asymptotic behavior. *Phys. Rev. A* **1988**, *38*, 3098–3100. [[CrossRef](#)]
33. Becke, A.D. Density-functional thermochemistry. IV. A new dynamical correlation functional and implications for exact-exchange mixing. *J. Chem. Phys.* **1996**, *104*, 1040–1046. [[CrossRef](#)]
34. Lee, C.; Yang, W.; Parr, R.G. Development of the Colle-Salvetti correlation-energy formula into a functional of the electron density. *Phys. Rev. B* **1988**, *37*, 785–789. [[CrossRef](#)] [[PubMed](#)]
35. Krishnan, R.; Binkley, J.S.; Seeger, R.; Pople, J.A. Self-consistent molecular orbital methods. XX. A basis set for correlated wave functions. *J. Chem. Phys.* **1980**, *72*, 650–652. [[CrossRef](#)]
36. Gill, P.M.W.; Johnson, B.G.; Pople, J.A.; Frisch, M.J. The performance of the Becke–Lee–Yang–Parr (B–LYP) density functional theory with various basis sets. *Chem. Phys. Lett.* **1992**, *197*, 499–505. [[CrossRef](#)]
37. Peng, C.; Schlegel, H.B. Combining Synchronous Transit and Quasi-Newton Methods to Find Transition States. *Isr. J. Chem.* **1993**, *33*, 449–454. [[CrossRef](#)]
38. Fukui, K. The path of chemical reactions—The IRC approach. *Acc. Chem. Res.* **1981**, *14*, 363–368. [[CrossRef](#)]

**Sample Availability:** Small samples (a few milligrams) of the compounds **8**, **12**, and **13** are available from the authors.

**Publisher’s Note:** MDPI stays neutral with regard to jurisdictional claims in published maps and institutional affiliations.



© 2020 by the authors. Licensee MDPI, Basel, Switzerland. This article is an open access article distributed under the terms and conditions of the Creative Commons Attribution (CC BY) license (<http://creativecommons.org/licenses/by/4.0/>).